Int. J. Heat Mass Transfer. Vol. 37, No. 2, pp. 257–268, 1994
Printed in Great Britain

0017–9310/94 $6.00 + 0.00

Thermophoretic transport with application to external vapor deposition processes

H. C. TSAI and R. GREIF
Department of Mechanical Engineering, University of California at Berkeley, Berkeley, CA 94720, U.S.A.

(*Received* 5 *January* 1993 *and in final form* 15 *June* 1993)

Abstract—A study has been made of the flow, heat transfer and thermophoretic transport with application to external vapor deposition processes. In this work the system studied consists of a jet emerging from a burner containing silica soot particles that are impinging on a disk which serves as the target for the depositing material. The motion of the particles is determined from the combined effects of thermophoresis, buoyancy and the forced flow. The governing conservation equations, which include the effects of buoyancy, variable properties and thermophoretic transport have been solved numerically. The effects of the particle distribution at the exit from the burner, the burner location, and the disk dimensions on particle deposition are studied. The local and average particle deposition and heat fluxes and the variation of the deposition efficiency are investigated over a range of values of the parameters.

1. INTRODUCTION

THE FABRICATION of high quality, low loss optical fibers has been successfully achieved by utilizing chemical vapor deposition processes (Li [1]). In the outside vapor deposition (OVD) and the vapor axial deposition (VAD) processes, silica particles are formed by passing a reacting vapor stream through a flame. The particles are directed towards and deposit on a target (Morrow *et al.* [2], Miizeki *et al.* [3]). Homsy *et al.* [4] and Batchelor and Shen [5] analyzed the thermophoretic deposition of particles in a uniform flow past a cylinder based on the Blasius series solution. Garg and Jayaraj [6, 7] calculated thermophoretic deposition over a cylinder in numerical studies specifying the pressure gradient of the external flow. These studies utilized the boundary layer assumptions with simple external flows. However, experimental results (Bautista *et al.* [8], Graham and Alam [9]) showed that the circumferential variation of the flow and heat transfer, as well as the interaction between the torch and the boule, have strong effects on the particle deposition. Numerical and experimental studies of particle deposition on a cylindrical target were carried out by Kim and Kim [10, 11]; deposition rates were obtained for TiO_2 particles as a function of particle diameter, flow Reynolds number and wall/gas temperature ratio at different angular positions along the upstream surface of the cylinder. Kang and Greif [12] numerically investigated the thermophoretic transport for an impinging jet on a cylinder and included the effects of buoyancy and variable properties. It is noted that the OVD and VAD processes entail complex flow, heat and mass transfer patterns in respect to the deposition on cylindrical targets.

To investigate deposition for a basic configuration, experiments were carried out by Hwang and Daily [13, 14] on the flame-synthesized silica particle deposition on a disk. The electric field enhancement of deposition was also studied [13, 14]. Relevant numerical studies have been carried out by Gokoglu and Rosner [15, 16] who analyzed the thermophoretic mass transfer on a cold plate, by Alam *et al.* [17, 18] who investigated thermophoretic deposition for a plane or slot jet impinging on a flat plate and by Evans and Greif [19] who studied the flow and heat transfer in respect to a rotating disk reactor.

In the present work a study is made of a high temperature, variable property air flow which contains particles that have formed at the exit from a burner. The flow and particles are transported towards a disk where deposition takes place. The buoyant jet which emerges from the burner is assumed to be laminar and steady. A finite volume numerical method is used to discretize and solve the coupled mass momentum and energy conservation equations; the concentration equation is then solved to determine the deposition rate. The effects of the particle distribution and the target configuration, including the disk diameter and the distance between the burner and the disk, are studied relative to particle deposition.

2. ANALYSIS

2.1. *Configuration and assumptions*

A buoyant, high temperature flow laden with fine soot particles emerges from a burner and impinges on a target (Fig. 1). In analyzing the phenomena the following assumptions have been made:

(1) The properties of the fluid vary with temperature.

(2) The flow is assumed to be laminar. The range of values of the Reynolds numbers based on the diam-

NOMENCLATURE

A_i	convection–diffusion coefficients
b	source term in the discretized equation
C	mass concentration of the particle
$\bar{C}$	average mass concentration of the particle
C_{peak}	peak mass concentration of the particle
C_f	skin friction coefficient, $2\tau_w/\rho_j\bar{u}_j^2$
c_p	specific heat at constant pressure
D	diameter of the disk
g	gravity
i, j	Cartesian base vector
J	local particle deposition flux
J^*	non-dimensional local particle deposition flux
$\bar{J}$	average particle deposition flux
$\bar{J}^*$	non-dimensional average particle deposition flux
K	coefficient of the thermophoretic velocity
k	conductivity
L	distance between the burner and the disk
p	static pressure
Re	Reynolds number, $\rho_j\bar{u}_jD/\mu_j$
S_ϕ	source term in the discretized differential equation
T	temperature
U^i	gas velocity
u, v	gas velocity in the x, r direction
u_{eff}, v_{eff}	particle velocity in the x, r direction
u_{th}, v_{th}	thermophoretic velocity in the x, r direction
w	radius of the burner
w_c	characteristic length of the Gaussian distribution
x, r	cylindrical coordinates.

Greek letters

Γ	general diffusivity
η	deposition efficiency
μ	viscosity
ξ^i	coordinates [$\xi^1 = x$, $\xi^2 = r$]
ρ	density
τ_w	shear stress at wall
ϕ	general dependent variable.

Subscripts

N, S, E, W	four nodes around the grid point P
a	ambient value
j	values at the burner exit
w	values at the wall.

eter of the nozzle, is from 100–1000 which is below the value for the onset of turbulence (Tennekes and Lumley [20]).

(3) The chemical reactions are assumed to be completed at the exit of the burner.

(4) The particle deposition mechanism has been established as resulting from thermophoresis; i.e. from the motion of a particle in a nonisothermal medium in the direction of decreasing temperature (Simpkins *et al.* [21], Walker *et al.* [22]). Particle deposition due to molecular diffusion is much smaller that that due to thermophoresis and is neglected [4, 5, 21, 22].

(5) The particles are smaller than one micron and the concentration is dilute; in the absence of thermophoresis, the particles would follow the gas flow [18, 19].

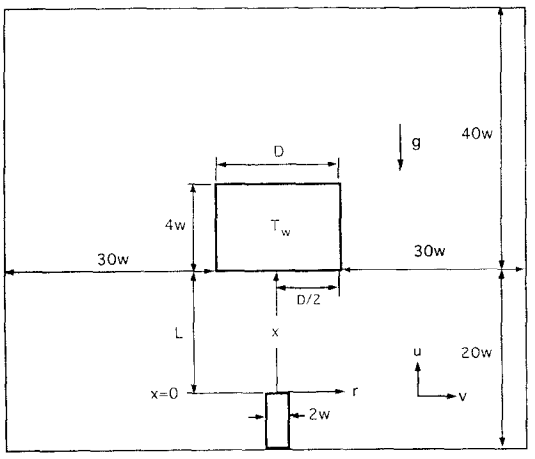

FIG. 1. Configuration and computational domain.

2.2. *Governing equations and boundary conditions*

Based on the above assumptions the conservation equations for mass, x-momentum, r-momentum, energy and particle concentration for the axially-symmetric round jet are written in the cylindrical coordinate system (x, r) as follows:

$$\frac{\partial}{\partial x}(\rho u) + \frac{\partial}{r\partial r}(r\rho v) = 0 \tag{1}$$

$$\rho u\frac{\partial u}{\partial x} + \rho v\frac{\partial u}{\partial r} = -\frac{\partial p}{\partial x} + \frac{\partial}{\partial x}\left(2\mu\frac{\partial u}{\partial x}\right) + \frac{\partial}{r\partial r}\left[r\mu\left(\frac{\partial u}{\partial r} + \frac{\partial v}{\partial x}\right)\right] - \rho g \tag{2}$$

$$\rho u\frac{\partial v}{\partial x} + \rho v\frac{\partial v}{\partial r} = -\frac{\partial p}{\partial r} + \frac{\partial}{\partial x}\left[\mu\left(\frac{\partial v}{\partial x} + \frac{\partial u}{\partial r}\right)\right] + \frac{\partial}{r\partial r}\left(2r\mu\frac{\partial v}{\partial r}\right) - \frac{2\mu v}{r^2} \tag{3}$$

$$\rho c_p u \frac{\partial T}{\partial x} + \rho c_p v \frac{\partial T}{\partial r} = \frac{\partial}{\partial x}\left(k \frac{\partial T}{\partial x}\right) + \frac{\partial}{r \partial r}\left(rk \frac{\partial T}{\partial r}\right) \quad (4)$$

$$\frac{\partial}{\partial x}(\rho u_{\text{eff}} C) + \frac{\partial}{r \partial r}(\rho v_{\text{eff}} C) = 0. \quad (5)$$

The velocities of the particles, $u_{\text{eff}} = u + u_{\text{th}}$, $v_{\text{eff}} = v + v_{\text{th}}$, equal the sum of the convective and thermophoretic velocities. The thermophoretic velocity is given by (Talbot *et al.* [23])

$$u_{\text{th}} = -K \frac{v}{T}\left(\frac{\partial T}{\partial x}\right), \quad v_{\text{th}} = -K \frac{v}{T}\left(\frac{\partial T}{\partial r}\right) \quad (6)$$

with K equal to 0.55 (Kim and Pratsinis [24]). The density, ρ, dynamic viscosity, μ, and conductivity, k, vary with temperature according to:

$$\frac{\rho}{\rho_a} = \left(\frac{T}{T_a}\right)^{-1}, \quad \frac{k}{k_a} = \left(\frac{T}{T_a}\right)^{p}, \quad \frac{\mu}{\mu_a} = \left(\frac{T}{T_a}\right)^{q} \quad (7)$$

where for air, $p = 0.785$ and $q = 0.673$ (Cebeci and Bradshaw [25]).

The boundary conditions imposed on equations (1)–(5) are given by (cf. Fig. 1):

(1) Disk: $u = 0$, $v = 0$, $T = T_w$. To determine the concentration of the particles at the surface of the disk, $C(x = L, r)$, the following expression, utilizing boundary layer theory and the ideal gas law is derived (Kang and Greif [12]):

$$\frac{C'(x = L, r)}{C(x = L, r)} \equiv \frac{C'_w}{C_w} = (p - q)\frac{T'_w}{T_w}; \quad (8)$$

where $\{\}'$ denotes the partial derivative with respect to the x coordinate which is normal to the surface.

(2) Burner exit: $x = 0$, $u_j(x = 0, r) = 2\bar{u}_j[1 - (r/w)^2]$, $v = 0$, $T = T_j$; $2w$ is the diameter of the jet at the burner exit. Two distributions for the particle mass concentration, $C(0, r)$, are used; namely

$$C(0, r) = C_{\text{peak}} \exp[-(r/w_c)^2 \ln 2] \quad (9a)$$

and

$$C(0, r) = \text{constant} = C(0) \quad (9b)$$

where C_{peak} is the peak concentration and w_c is the characteristic width of the particle distribution at the burner exit. For the Gaussian normal distribution, equation (9a), the average particle mass concentration is given by $\bar{C}(0) = C_{\text{peak}}(w_c/w)^2[1 - \exp(-(w/w_c)^2 \ln 2)]/\ln 2$. The Gaussian normal distribution in equation (9a) suggested by Bautista *et al.* [26] is consistent with the injection of silicon tetrachloride at the center of the burner. The uniform distribution, which is closer to a twin-peak distribution, is also examined in this study.

(3) Side walls of burner; $u = 0$, $v = 0$, $\partial T/\partial r = 0$, $\partial C/\partial r = 0$.

(4) Upstream entrained region: $\partial u/\partial x = 0$, $\partial v/\partial x = 0$, $T = T_a = 300$ K, $C = 0$.

(5) Outer entrained region: $\partial u/\partial r = 0$, $\partial(rv)/r\partial r = 0$, $T = T_a = 300$ K, $C = 0$.

(6) Far downstream region: $\partial^2 u/\partial x^2 = 0$, $\partial v/\partial x = 0$, $\partial^2 T/\partial x^2 = 0$, $\partial^2 C/\partial x^2 = 0$.

2.3. *Deposition flux*

The local particle deposition flux, $J(x = L, r) \equiv J(r)$, is obtained from the product of the axial component of the thermophoretic velocity, $\mu_{\text{th,w}}$, and the particle mass concentration, C_w, at the wall:

$$J(x = L, r) \equiv J(r) = u_{\text{th,w}} C_w,$$

$$J^*(x = L, r) \equiv J^*(r) = \frac{J(r)}{\bar{u}_j \bar{C}(0)}. \quad (10)$$

The average particle deposition flux, $\bar{J}(x = L) \equiv \bar{J}$, is given by

$$\bar{J}(x = L) \equiv \bar{J} = \frac{8}{D^2}\int_0^{D/2} u_{\text{th,w}} C_w r \, dr,$$

$$\bar{J}^*(x = L) \equiv \bar{J}^* = \frac{\bar{J}}{\bar{u}_j \bar{C}(0)} \quad (11)$$

where D is the diameter of the disk. The deposition efficiency η is defined as the ratio of the total deposition rate, $\bar{J}\pi D^2/4$, to the incident mass flow rate of the particles:

$$\eta = \frac{\int_0^{D/2} Jr \, dr}{\int_0^{w} u_j(0, r) C(0, r) r \, dr} = \frac{\bar{J} D^2}{8\int_0^{w} u_j(0, r) C(0, r) r \, dr}. \quad (12)$$

3. NUMERICAL METHOD

3.1. *Numerical procedure*

The governing equations (1)–(4) can be written in the following conservative form:

$$\frac{\partial}{\partial \xi^i}\left(\rho U^i \phi - \Gamma \frac{\partial \phi}{\partial \xi^i}\right) - b = 0 \quad i, j = 1, 2 \quad (13)$$

which admits a common solution procedure. Here ϕ denotes a dependent variable, b is the general source term, ξ^i denotes the coordinates, U^i denotes the velocity and Γ is the diffusivity. It is noted that for the concentration equation for the particles, equation (5), that Γ and b are both set equal to zero. The calculation of the pressure proceeds according to the SIMPLE algorithm of Patankar [27] by making corrections at each iteration, until the velocities and the corrected pressure field satisfy the coupled continuity and momentum equations. A non-staggered grid system is chosen for simplicity in complicated configurations; all dependent variables are calculated and stored at the same intersection of grid lines rather than at staggered grid locations. To minimize difficulties with the

determination of the pressure field, the velocities (on the surfaces of the control volume) are determined differently; i.e. they are obtained by solving linearized momentum equations (Schuh [28]). The imposed boundary conditions for the pressure correction equation are given by the components of the momentum equations which are normal to the boundary surfaces (Gresho and Sani [29]).

To minimize oscillations resulting from higher order schemes, the HYBRID scheme is adopted (Patankar [27]) to linearize the convective terms for moderate Reynolds numbers. A central difference representation is used for the diffusion term. The quantity S_ϕ includes all the terms proportional to the control volume. The discretized form of the differential equation is obtained by the finite volume method (Patankar [27]) and is written as

$$A_P\phi_P = A_N\phi_N + A_S\phi_S + A_E\phi_E + A_W\phi_W + S_\phi. \quad (14)$$

The coefficients A_i are obtained by integrating the convective and diffusive fluxes over the control surfaces and the subscripts N, S, E and W denotes the four neighboring grid points around P.

To solve the discretized linear equations, the Generalized Minimum Residual method (GMRES) (Saad and Schultz [30]) with Incomplete Lower and Upper triangle matrix decomposition (ILU) preconditioning is adopted, because of its robustness and fast convergence. The solution procedure is iterative in nature. The criterion used for convergence is that the sum of the dimensionless residuals over the entire domain is less than 10^{-5} for every equation. In addition, it is also required that the relative change of each dependent variable is less than 0.01% for each iteration.

3.2. *Validation*

The numerical code was first used to solve benchmark type problems; namely, steady, buoyant flow in a square enclosure with the vertical surfaces at different temperatures and the horizontal surfaces insulated. The velocity and Nusselt number distributions were in excellent agreement with the results of de Vahl Davis [31] for a range of Rayleigh numbers from 10^4 to 10^6. In addition, the problem of a laminar non-buoyant jet impinging on an infinite flat disk (Aihara *et al.* [32]) was also solved. Excellent agreement for the skin friction, pressure coefficient and Nusselt number was achieved for this problem.

3.3. *Computational domain, grid alignment and grid dependency*

Referring to Fig. 1, the upstream and downstream locations are fixed at $-20w$ and $+40w$, respectively. The lateral region extends from $-30w-D/2$ and

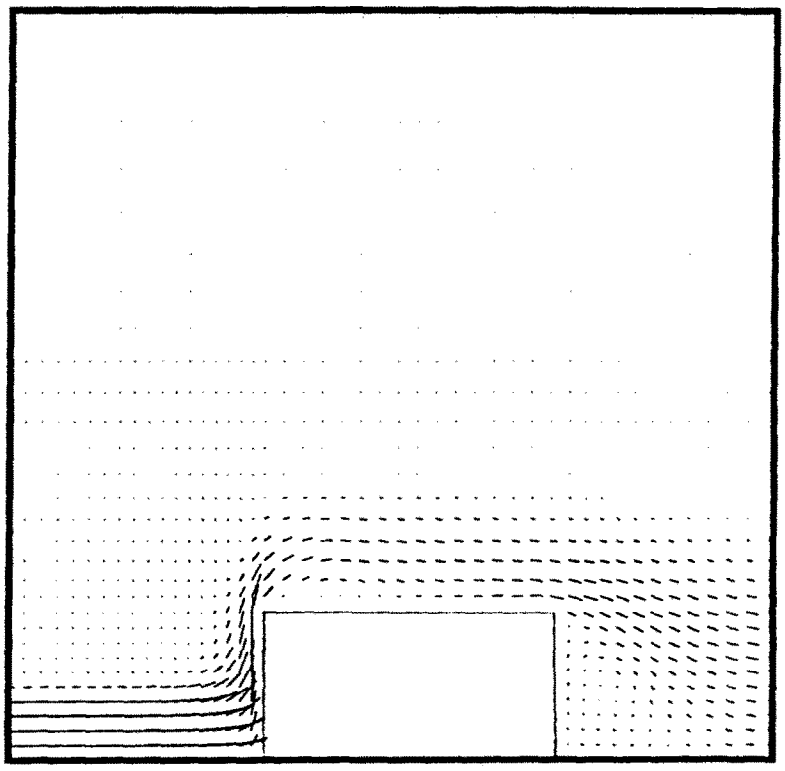

FIG. 2(a). Velocity vectors in a x–r plane; $D = 6$ cm, $L = 13$ cm, $Re = 380$.

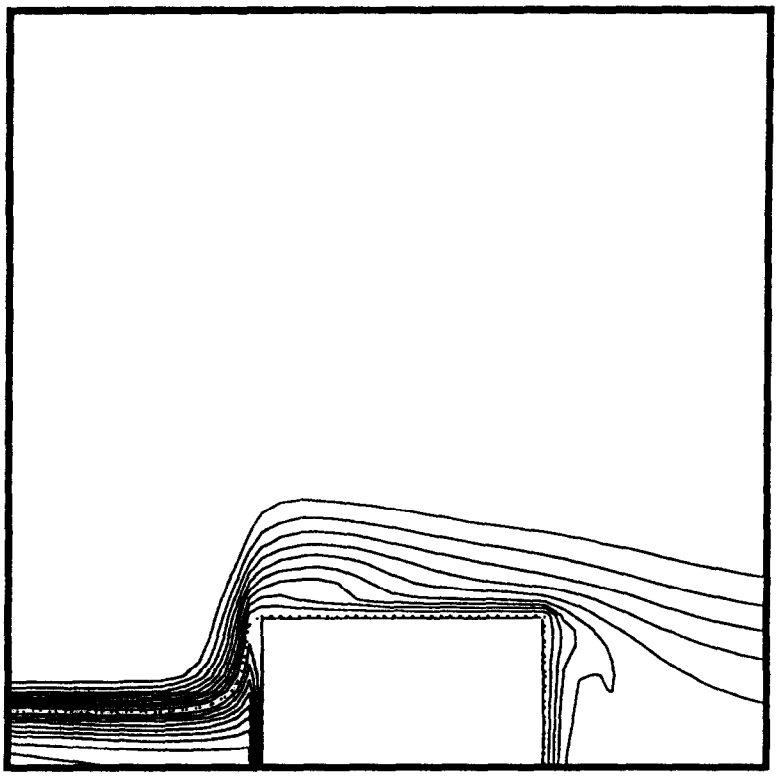

FIG. 2(b). Isothermal contours in a x–r plane; $D = 6$ cm, $L = 13$ cm, $Re = 380$.

$+30w+D/2$. The validity of the computational domain has been checked by increasing the dimensions of the domain by 20%. For this case the results for the skin friction coefficient and Nusselt number change by less than 1%. The length and diameter of the burner, and the length of the disk, are $9w$, $2w$ and $4w$, respectively. The burner is centered on the target and the distance between the burner exit and the target is $8.7w$.

Typical grids in (x, r) coordinates were 121×81, which was checked to insure grid independent results. For the case $D = 6$ cm and $\bar{u}_j = 3$ m s^{-1}, i.e. $Re = 360$, increasing the grids to 141×81, changed the local shear stress and heat fluxes by 0.1 and 0.07%, respectively. By decreasing the grids to 101×81, the results changed by 0.5%. Increasing the grids to 121×121, the local shear stress and heat flux on the wall changed by 0.1 and 0.1%, respectively. Decreasing the grids to 121×61, the corresponding results changed by 1.0 and 0.9%, respectively. To achieve high accuracy in the region near the target surface and burner exit the first grid size is $0.005w$ and the grid sizes then increase by 10% with increasing distance.

4. RESULTS AND DISCUSSION

4.1. *Flow and heat transfer*

The velocity and temperature fields and the local heat flux are obtained from the solution of equations (1)–(4) and the associated boundary conditions. The temperature, T_j, and the average velocity, u_j, of the jet at the burner exit, are fixed at 2300 K and 3 m s^{-1}, respectively. The temperature of the disk, T_w, is fixed at 1300 K. The diameter of the burner, $2w$, is 3 cm; the diameter of the disk, D, is varied from 3 to 9 cm; the thickness of the disk is 6 cm. The Reynolds number, Re $(=\rho_j \bar{u}_j D/\mu_j)$, is varied from 190 to 570. The distance between the exit from the burner and the disk, L, is varied from 3.25 to 13 cm.

The velocity vectors and the isothermal contours are shown in Figs. 2(a), (b) and 3(a), (b) for $D = 6$ and 9 cm ($Re = 380$ and 570) and $L = 13$ cm. The flow pattern for the development of the buoyant jet may be considered to include free jet, stagnation, wall jet, near and far wake regions. The upstream region essentially corresponds to a developing free jet with a small pressure gradient. The flow impinges on the disk and separates upon turning around the front edge of the disk. Recirculation occurs along the sides and rear of the disk. It is seen that when the disk diameter is increased, the larger blockage results in larger recirculation regions. The driving pressure for the flow diminishes along the surface; lower pressures result downstream and the recirculation regions are larger and convection is diminished. Note that the temperature contours marked by the dashed curves shown in Figs. 2(b), 3(b) are equal to the temperature of the disk.

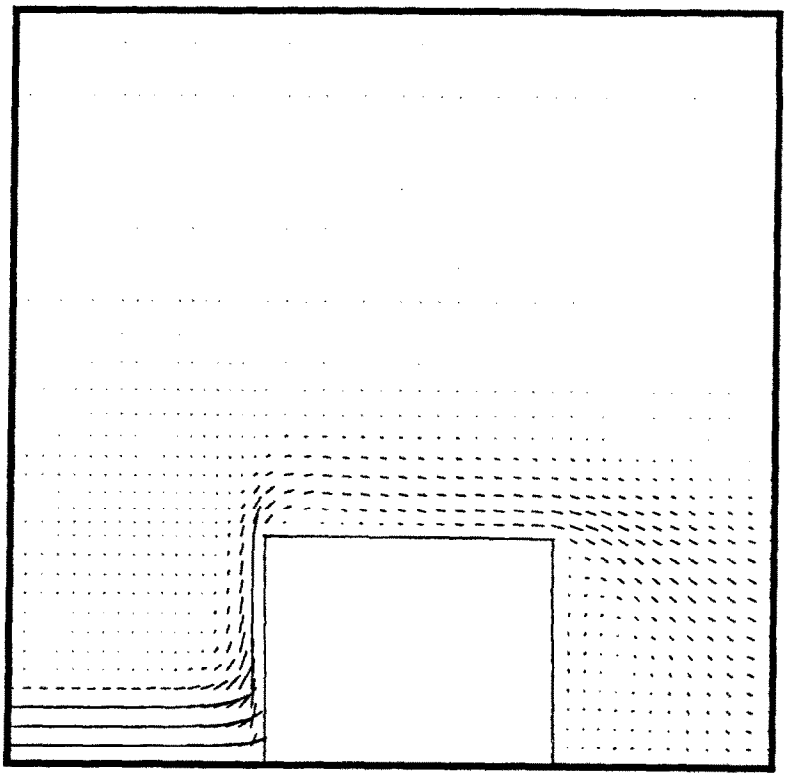

FIG. 3(a). Velocity vectors in a x–r plane: $D = 9$ cm, $L = 13$ cm, $Re = 570$.

The results for the friction and the heat transfer, are shown in Figs. 4(a), (b). The variation of the friction coefficient, $C_f(=2\tau_w/\rho_j\bar{u}_j^2)$, along the surface is presented for three disk diameters in Fig. 4(a). For all of the disks, the friction coefficient increases for increasing radial locations over the range $0 < r < 1.5$ cm; note that the radius of the jet at the burner exit is $r = 1.5$ cm. For disk radial locations greater than approximately 1.5 cm, the friction coefficients decrease radially. Note that the friction increases for decreasing disk diameters. In Fig. 4(b), the local heat transfer coefficient, h, is presented for three disk diameters. In the central stagnation region, the heat transfer is highest. Furthermore, the heat transfer increases for decreasing disk diameters.

4.2. *Effects of particle distribution and disk size on deposition*

To study the effects of the particle distribution on deposition, both the Gaussian and the uniform particle mass concentration distributions, equations (9a) and (9b), were considered. Note that the special case of the Gaussian distribution with the characteristic length $w_c = \infty$ also corresponds to the uniform distribution. Four values of w_c have been used: $w_c = 0.5$, 0.75, 1.0, ∞ (cm). Disk diameters of 3, 4.5, 6, 7.5 and 9 cm and distances between the burner and the disk, L, of 3.25, 6.5 and 13 cm are studied. The deposition is proportional to the average particle mass concentration, $\bar{C}(0)$, so that the dimensionless deposition fluxes, $J^*(r)$ or $\bar{J}^*$, are independent of $\bar{C}(0)$.

The effects of the particle distribution on the local particle deposition flux, $J^*(r)$, are shown in Fig. 5(a) for a disk diameter, D, of 6 cm, and $L = 13$ cm. It is seen that when w_c increases, corresponding to a more uniform distribution, the particle deposition flux is also more uniform but is smaller in magnitude. The particles moving near the center line experience stronger thermophoretic forces (near the disk) due to the larger temperature gradient (in the direction normal to the target surface) at the center line. Thus, when more of the particles are present near the center, corresponding to the distribution for smaller w_c, the particle deposition is larger. It is noted that the uniformity and magnitude of the deposition flux are essential factors in achieving successful CVD processes. It is shown that the particle distribution, which is determined by the burner, has an important influence on particle deposition.

The deposition distribution along the disk, J^*, for $D = 3$, 6 and 9 cm, and $L = 13$ cm, are shown in Figs. 5(b), (c) for $w_c = 0.75$ and $w_c = \infty$, respectively. Over most regions, the smaller disks result in larger deposition. Referring to the heat transfer results presented in Fig. 4(b), the smaller disks result in larger heat transfer (larger thermophoretic forces). However, the

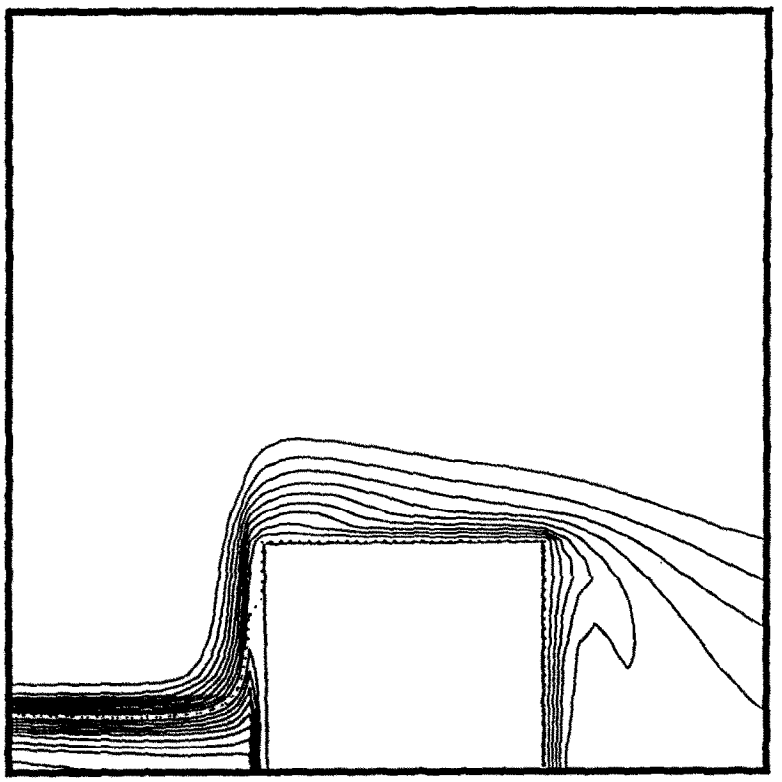

FIG. 3(b). Isothermal contours in a x–r plane; $D = 9$ cm, $L = 13$ cm, $Re = 570$.

particle velocities parallel to the surface are larger for the smaller disks. These effects oppose one another in respect to deposition. For the cases studied, the results show that the thermophoretic force dominates and the deposition increases for the smaller disks.

Figure 6(a) shows the results for the average deposition flux, $\bar{J}^*$, as a function of disk diameter for the four characteristic distribution lengths, w_c, and $L = 13$ cm. For the smaller disk diameters, the average deposition fluxes are larger (in accord with the discussion above for the local deposition fluxes). In respect to the particle distribution, a more uniform distribution; i.e. larger w_c, results in the passage of more particles around the target and thus smaller values of $\bar{J}^*$. In contrast, a non-uniform distribution with a greater number of particles near the center line, benefits from the larger temperature gradient near the center line and results in larger particle deposition (as discussed above for the local flux $J^*(r)$).

The deposition efficiency, η, as a function of disk size is shown in Fig. 6(b) for the four particle distributions and $L = 13$ cm. For a given distribution (fixed w_c) the larger disks result in greater deposition efficiency. When the disk diameter exceeds 6 cm, the deposition efficiency for a given distribution is approximately constant because there is little deposition in the region, $r > 0.03$ m (see Figs. 5(b), (c) for the $D = 0.09$ m case). The more non-uniform particle distributions: i.e. smaller w_c, result in greater deposition efficiencies.

For a given distance between the burner and the target, L, and a given jet velocity, $\bar{u}_j$, the average deposition flux $\bar{J}$ may be correlated in the form $\bar{J} \sim \bar{C}(0)D^m$; i.e. $\bar{J}^* \sim D^m$. It is pointed out that all of the calculations have been made for a jet velocity, $\bar{u}_j$, of 3 m s^{-1}. As noted above, for a given distribution the results in Fig. 6(b) yield for $D > 6$ cm that $\eta =$ constant so that $\bar{J}D^2 =$ constant or $\bar{J} \sim D^{-2}(m = -2)$; the results for smaller diameters (Fig. 6(b)) may be approximated by $\bar{J}D^2 \sim D$, or $\bar{J} \sim D^{-1}$. There is a transition range between these 'limiting' results.

4.3. *Effect of distance between burner and target*

Figure (7) shows the variation of the local deposition flux, $J^*(r)$, for the particle distribution $w_c = 0.75$. The results are for three distances between the burner and the target; i.e. for $L = 3.25$, 6.5 and 13 cm for a disk diameter of 6 cm. The smaller values of L result in larger values for the deposition flux but have a slightly more non-uniform distribution.

Results for the average particle deposition flux, $\bar{J}^*$, as a function of the distance L, for the particle distributions $w_c = 0.5$, 0.75, 1.0 and ∞ cm, for $D = 6$ cm, are shown in Fig. 8(a); the results for the deposition efficiency, η, are shown in Fig. 8(b). The results show

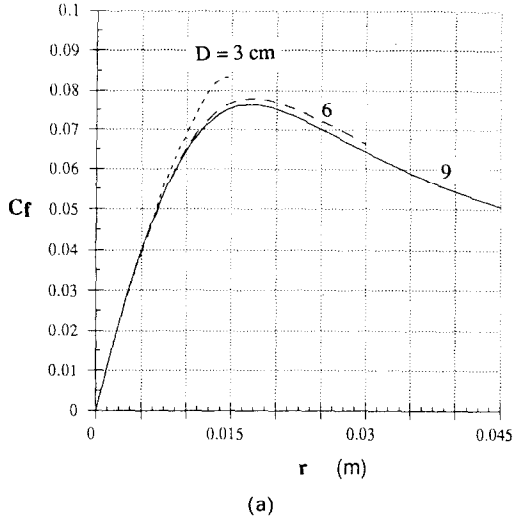

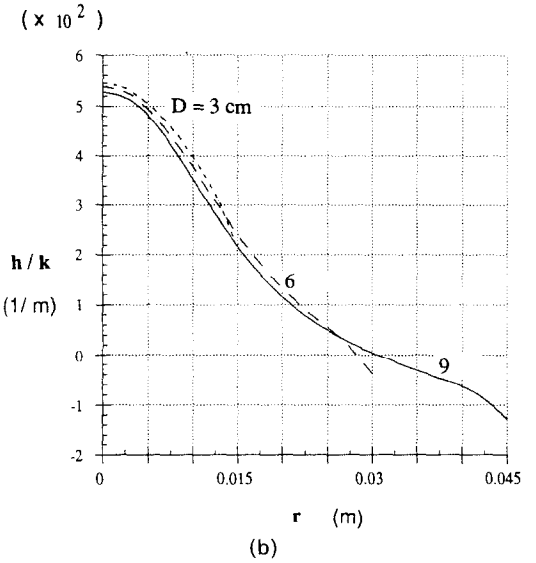

FIG. 4. (a) Variation of the friction coefficient along the surface, effect of D; $L = 13$ cm. (b) Variation of the heat transfer coefficient along the surface, effect of D; $L = 13$ cm.

that the shortest distance, $L = 3.25$ cm (greatest blockage), yields the greatest deposition. In addition, the acceleration of the free jet due to buoyancy is limited for a short distance L. The resulting smaller velocities for the small L case cause the friction along the surface to be smaller for $r < 0.015$ m as shown in Fig. 9(a) for $D = 6$ cm and $w_c = 0.75$ (but larger values are obtained at large radial locations). The increased heat transfer shown in Fig. 9(b) indicates larger thermophoretic velocities for the smaller L cases. Both of these effects contribute to the increased deposition.

4.4. *Study of Hwang and Daily* [13, 14]

Hwang and Daily [13, 14] carried out an investigation of the deposition of silica on disks. Gas flows of methane, nitrogen, oxygen and silicon tetrachloride were delivered to a burner which consisted of eight

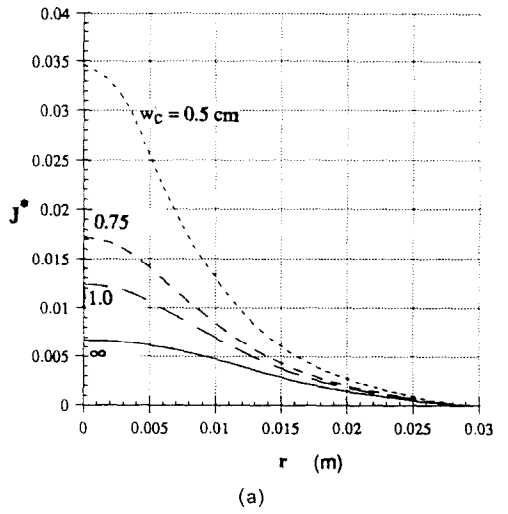

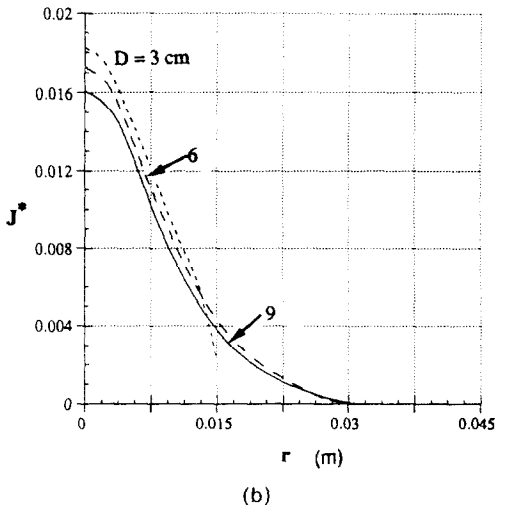

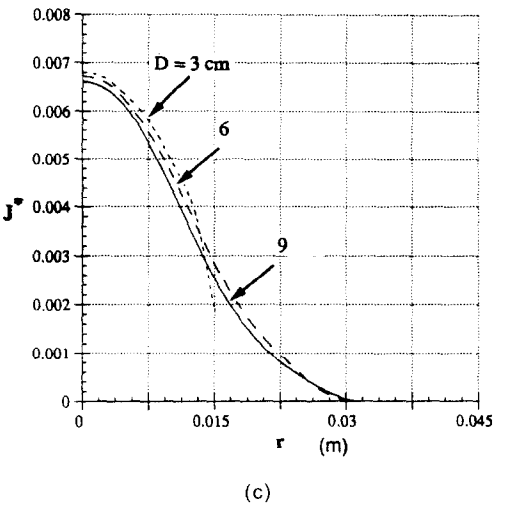

FIG. 5. (a) Variation of the particle deposition flux along the surface, effect of w_c; $D = 6$ cm, $L = 13$ cm. (b) Variation of the particle deposition flux along the surface, effect of D; $w_c = 0.75$ cm, $L = 13$ cm. (c) Variation of the particle deposition flux along the surface, effect of D; $w_c = \infty$ cm, $L = 13$ cm.

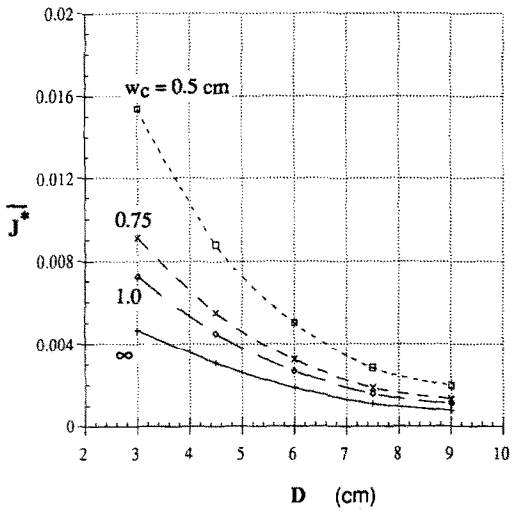

(a)

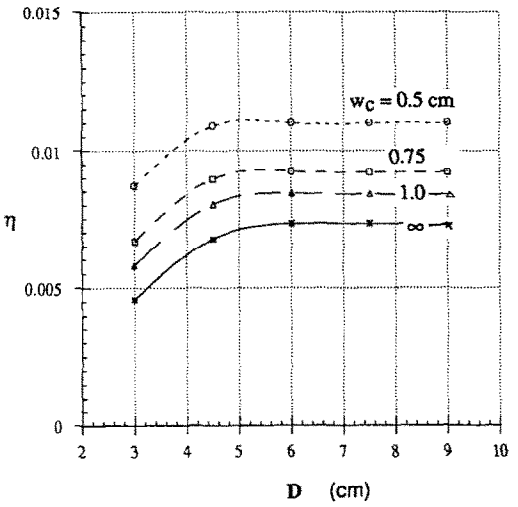

(b)

FIG. 6. (a) Variation of the average deposition flux with disk diameter, effect of w_c; $L = 13$ cm. (b) Variation of the deposition efficiency with disk diameter, effect of w_c; $L = 13$ cm.

concentric tubes utilizing a design of Bautista *et al.* [26]. The combustion of methane resulted in the high temperatures required for the hydrolysis and oxidation of silicon. Temperature distributions were measured at the burner exit and in the gas stream by using thermocouples. Measurements were made of the mass of silica deposited on the disks and of the silicon tetrachloride consumed. Four disks of different diameters ranging from 4.5 to 9 (cm) were used to study the deposition of silica soot particles.

† In reference to the comments of the referee: (1) it is felt that the important effects of variable properties are partially responsible for the difference in the results obtained from the present numerical study and from the previous predictions and (2) the present formulation has yielded good agreement for many published flows [12].

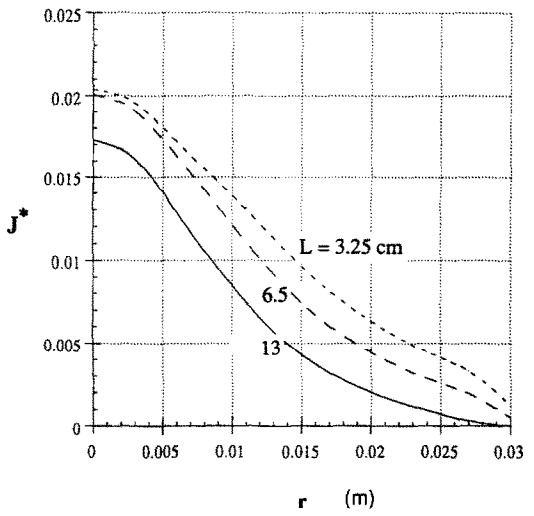

FIG. 7. Variation of the local deposition flux along the surface, effect of L, $w_c = 0.75$; $D = 6$ cm.

Hwang and Daily [13, 14] report that their experimental data resulted in an average deposition flux, $\bar{J}$, that is proportional to $D^{-0.5}$ while the present calculations give $\bar{J} \sim D^{-2}$ for $D > 6$ cm. It is pointed out that the present study does not account for chemical reactions that continue after the jet leaves the burner. These reactions result in an increase in the gas temperature and in the particle concentration outside the burner which are not accounted for in the calculations. These effects may be responsible for the differences between the predicted and the experimental results and future studies are planned to include these and related effects. Hwang and Daily [13, 14] show that the constant property, similarity solution for non-buoyant stagnation boundary layer flow on a disk of finite size yields $\bar{J} \sim D^{-0.5}$ which is in agreement with their experimental data. It is also noted that the experimental data of Bautista *et al.* [8] for the particle deposition on a cylindrical target resulted in a deposition flux that is proportional to (target diameter)$^{-0.5}$. Bautista *et al.* [8] utilized the constant property analytical solution of Homsy *et al.* [4] for a symmetrical surface and obtained $\bar{J} \sim D^{-0.5}$ which is in agreement with their experimental data.†

A direct numerical comparison may be made between the experimental results and the numerical predictions with the specification of the diameter, d_p, mass density, ρ_p, and average number density, $\bar{n}_p$, of the SiO_2 particles:

$$\bar{C}(0) = \frac{\pi d_p^3}{6} \rho_p \bar{n}_p. \tag{15}$$

There are significant variations in the values of these and related quantities (Bautista *et al.* [26], Flower and Hurd [33], Zachariah *et al.* [34], Allendorf and Palmer [35], Alendorf *et al.* [36]) which depend on burner type, flame configuration, test conditions, etc. Hwang and Daily [13, 14] obtain good agreement with their

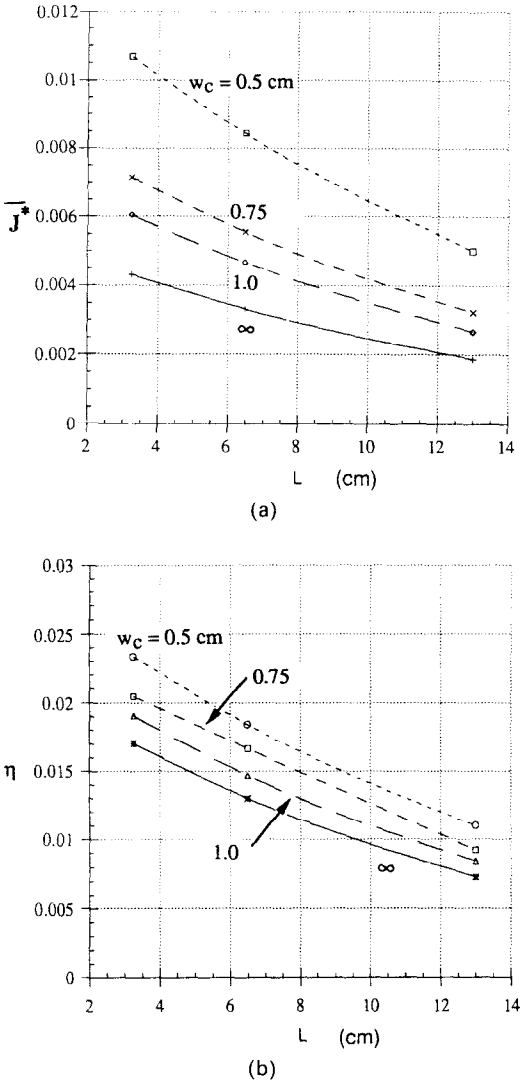

FIG. 8. (a) Variation of the average deposition flux with the distance between the burner and the target, effect of w_c; $D = 6$ cm. (b) Variation of the deposition efficiency with the distance between the burner and the target, effect of w_c; $D = 6$ cm.

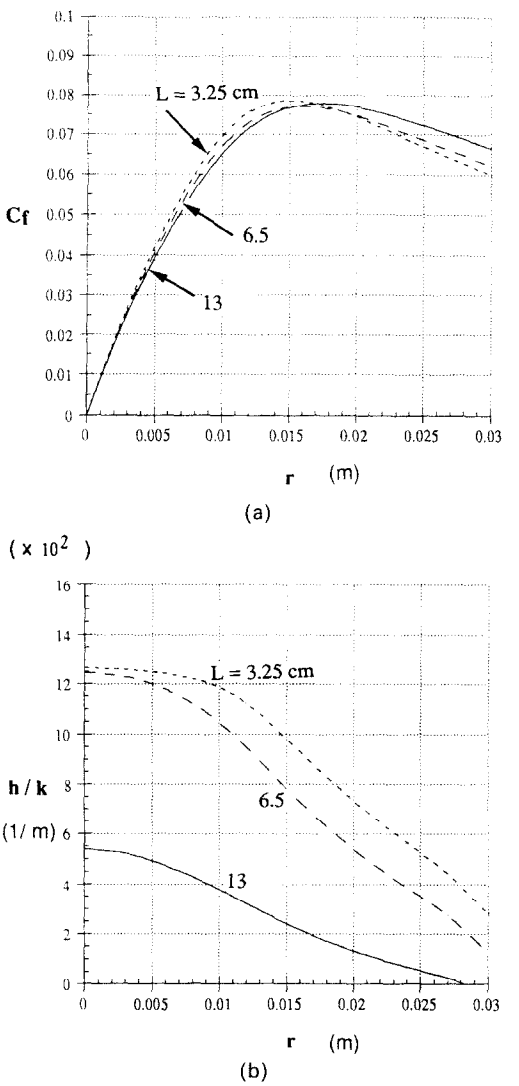

FIG. 9. (a) Variation of the friction coefficient along the surface, effect of L. (b) Variation of the heat transfer coefficient along the surface, effect of L.

experimental data with values of $\bar{u}_j = 3$ m s^{-1}, $L = 13$ cm, $d_p = 0.2$ μ m, $\rho_p = 2.2$ g cm^{-3} and $\bar{n}_p = 2$–4×10^9 (cm^{-3}); i.e. $\bar{C}(0) = 1.8$–3.7×10^{-5} (g cm^{-3}). Bautista *et al.* [8] obtained good agreement with their experimental data with $\bar{C}(0) = 2 \times 10^{-3}$ (g cm^{-3}). It is noted that in respect to the present calculations these values do not give agreement with the experimental data of Hwang and Daily [13, 14].

5. CONCLUSIONS

The Navier–Stokes, energy and concentration equations have been solved to predict the fluid flow, heat transfer and particle deposition on a disk. The effects of variable properties, buoyancy and thermophoresis have been included in the study. The following conclusions are drawn.

(1) When the diameter of the disk is increased, the increased blockage changes the flow and temperature fields, and results in larger recirculation regions. The skin friction coefficient and the local heat flux are reduced. The former results in a decrease in the velocity parallel to the surface which increases the thermophoretic transport while the latter results in a decrease in the thermophoretic transport. For the cases studied the results show that for increasing diameters the latter effect dominates and the average deposition flux decreases, although the deposition efficiency increases due to the larger area.

(2) The distribution of the particles at the burner exit has considerable influence on the deposition on

the disk. A non-uniform distribution, with a larger number of particles in the center, results in a larger but non-uniform deposition flux. A more uniform distribution, i.e. larger w_c, results in a smaller but more uniform deposition flux.

(3) For the cases studied, when the distance between the burner exit and the disk, L, is reduced, the larger thermophoretic force results in increased deposition. However, the deposition is more non-uniform in comparison to the case for larger L.

(4) The predictions for the deposition are not in agreement with the experimental data of Hwang and Daily [13, 14] which are correlated according to $\bar{J} \sim D^{-0.5}$. For the present calculations, for the four assumed Gaussian distributions with particle distributions characterized by $w_c = 0.5$, 0.75, 1.0 and ∞, and for disk diameters greater than 6 cm, the predictions give $\bar{J} \sim D^{-2}$. Future studies will include the effects of chemical reactions outside the burner which have been neglected in the present study.

Acknowledgement—Support from the National Science Foundation, the Pittsburgh and San Diego Supercomputer Centers, and the Computing Center of the University of California at Berkeley is gratefuly acknowledged. The research is part of a joint program with Professor J. W. Daily of the University of Colorado on chemical vapor deposition processes. The authors are indebted to Professors J. W. Daily, J. Hwang and S. H. Kang for helpful discussions.

REFERENCES

1. T. Li, *Optical Fiber Communications: Volume 1, Fiber Fabrication*. Academic Press, London (1985).
2. A. M. Morrow, A. Sarkar and P. C. Schultz, Outside vapor deposition. In *Optical Fiber Communications: Fiber Fabrication* (Edited by T. Li). Academic Press, London (1985).
3. N. Miizeki, N. Inagaki and T. Edahiro, Vapor-phase axial deposition method. In *Optical Fiber Communications: Volume 1. Fiber Fabrication* (Edited by T. Li). Academic Press, London (1985).
4. G. M. Homsy, K. L. Walker and F. T. Geyling, Blasius series for thermophoretic deposition of small particles, *J. Colloid Interface Sci.* **83,** 495–510 (1981).
5. G. K. Batchelor and C. Shen, Thermophoretic deposition of particles in gas flowing over cold surfaces, *J. Colloid Interface Sci.* **107,** 21–37 (1985).
6. V. K. Garg and S. Jayaraj, Thermophoretic deposition over a cylinder, *Int. J. Engng Fluid Mech.* **3,** 175–196 (1990).
7. V. K. Garg and S. Jayaraj, Thermophoretic deposition in crossflow over a cylinder, *J. Thermophys.* **4,** 115–116 (1990).
8. J. R. Bautista, K. L. Walker and R. M. Atkins, Modeling heat and mass transfer in optical waveguide manufacturing, *Chemical Engng Process* 47–52 (1990).
9. G. M. Graham and M. K. Alam, Experimental study of the outside vapor deposition process, *Aerosol Sci. and Tech.* **15,** 69–76 (1991).
10. Y. J. Kim and S. S. Kim, Numerical simulation of particle deposition onto a circular cylinder in non-isothermal two-phase cross flows, *ASME/JSME Thermal Engng Proceedings* **2,** 95–100 (1991).
11. Y. J. Kim and S. S. Kim, Experimental study of particle deposition onto a circular cylinder in high temperature particle-laden flows, *Experimental Thermal Sci.* **5,** 116–123 (1992).
12. S. H. Kang and R. Greif, Thermophoretic transport in the outside vapor deposition process, *Int. J. Heat Mass Transfer* **36,** 1007–1018 (1993).
13. J. Hwang and J. Daily, Electric field enhanced deposition in materials manufacturing: temperature and electric field measurements, submitted for publication.
14. J. Hwang, Flame deposition processes in materials manufacturing, Ph.D. Dissertation, University of California, Berkeley, Department of Mechanical Engineering (1991).
15. S. A. Gokoglu and D. E. Rosner, Viscous dissipation effects on thermophoretically augmented aerosol particle transport across laminar boundary layers, *Int. J. Heat Fluid Flow* **6,** 293–297 (1985).
16. S. A. Gokoglu and D. E. Rosner, Thermophoretically augmented mass transfer rates to solid walls across laminar boundary layers, *AIAA J.* **24,** 172–179 (1986).
17. M. K. Alam, G. Graham, V. Janakiraman and J. Greaves, Numerical analysis of thermophoretic transport in the OVD process, *Numer. Heat Transfer, ASME* **130,** 67–72 (1990).
18. M. K. Alam, G. Graham and V. Janakiraman, Particle transport by thermophoresis in a slot jet impinging on a wall, *Heat Transfer Effects in Materials Processing, ASME* **233,** 15–21 (1992).
19. G. Evans and R. Greif, A numerical model of the flow and heat transfer in a rotating disk chemical vapor deposition reactor, *Trans. of ASME J. Heat Transfer* **109,** 1063–1069 (1986).
20. H. Tennekes and J. L. Lumley, *A First Course in Turbulence*. MIT Press, Cambridge, MA (1972).
21. P. G. Simpkins, S. G. Kosinski and J. B. MacChesney, Thermophoresis: the mass transfer mechanism in modified chemical vapor deposition, *J. Appl. Phys.* **50,** 5676–5681 (1979).
22. K. L. Walker, G. M. Homsy and F. T. Geyling, Thermophoretic deposition of small particles in laminar tube flow, *J. Colloid Interface Sci.* **69,** 138–147 (1979).
23. L. Talbot, R. K. Cheng, R. W. Schefer and D. R. Willis, Thermophoresis of particles in a heated boundary layer, *J. Fluid Mech.* **101,** 737–758 (1980).
24. K. S. Kim and S. E. Pratsinis, Manufacture of optical waveguide preforms by modified chemical vapor deposition, *A.I.Ch.E. Jl* **34,** 912–920 (1988).
25. T. Cebeci and P. Bradshaw, *Physical and Computational Aspects of Convective Heat Transfer*. Springer, New York (1984).
26. J. R. Bautista, E. Potkay and D. L. Scatton, Particle size measurement in optical waveguide manufacturing torches using light scattering, *Material Research Society Symp. Proc.* **117,** 151–156 (1988).
27. S. V. Patankar, *Numerical Heat Transfer and Fluid Flow*. Hemisphere, New York (1980).
28. M. J. Schuh, Numerical prediction of fluid and particle motions in flows past tubes, PhD. Dissertation, University of California, Berkeley (1987).
29. P. M. Gresho and R. L. Sani, On pressure boundary condition for the incompressible Navier–Stokes equations, *Int. J. Numer. Meth. Fluids* **7,** 1111–1145 (1987).
30. Youcef Saad and Martin H. Schultz, GMRES: A generalized minimal residual algorithm for solving nonsymmetric linear systems, *SIAM J. Sci. Stat. Comput.* **7,** 856–869 (1986).
31. G. de Vahl Davis, Natural convection of air in a square cavity: a bench mark numerical solution, *Int. J. Numer. Meth. Fluids* **3,** 249–264 (1983).
32. T. Aihara, J. K. Kim and S. Maruyama, Effects of temperature-dependent fluid properties on heat transfer due to an axisymmetric impinging gas jet normal to a flat surface, *Wärme- und Stoffübertragung* **25,** 145–153 (1990).

33. W. L. Flower and A. J. Hurd, In situ measurement of flame-formed silica particles using dynamic light scattering, *Appl. Optics* **26,** 2236–2239 (1987).
34. M. R. Zachariah, D. Chin and H. G. Semerjian, Silica particles synthesis in a counterflow diffusion flame reactor, *Combust. Flame* **78,** 287–298 (1989).
35. M. D. Allendorf and R. E. Palmer, Spontaneous Raman spectroscopy in flames containing high concentrations of silica particles, *High Temp. Sci.* **26,** 45 (1990).
36. M. D. Allendorf, J. R. Bautista and R. E. Palmer, Temperature measurements in a vapor axial deposition flame by spontaneous Raman spectroscopy, *J. Appl. Phys.* **66,** 5046 (1990).